Effects of pre-treatment and plasma enhancement on chemical vapor deposition of carbon nanotubes from ultra-thin catalyst films

M. Cantoro [a,*], S. Hofmann [a], S. Pisana [a], C. Ducati [b], A. Parvez [a], A.C. Ferrari [a], J. Robertson [a]

[a] *Department of Engineering, University of Cambridge, Trumpington Street, Cambridge CB2 1PZ, UK*
[b] *Department of Materials Science and Metallurgy, University of Cambridge, Pembroke Street, Cambridge CB2 3QZ, UK*

Available online 28 February 2006

Abstract

We report a detailed study of surface-bound chemical vapor deposition of carbon nanotubes and nanofibers from evaporated transition metal catalysts exposed to ammonia diluted acetylene. We show that a reduction of the Fe/Co catalyst film thickness below 3 nm results into a transition from large diameter (>40 nm), bamboo-like nanofibers to small diameter (~ 5 nm) multi-walled carbon nanotubes. The nanostructuring of ultra-thin catalyst films critically depends on the gas atmosphere, with the resulting island distribution initiating the carbon nucleation. Compared to purely thermal chemical vapor deposition, we find that, for small diameter nanotube growth, DC plasma assistance is detrimental to graphitization and sample homogeneity and cannot prevent an early catalyst poisoning.
© 2006 Elsevier B.V. All rights reserved.

Keywords: Nanotubes; Nanofibers; Chemical vapor deposition; Plasma CVD

1. Introduction

Catalytic chemical vapor deposition (CVD) has the unique advantage of allowing bulk production and selective, aligned growth of individual carbon nanotubes (CNTs) and nanofibers (CNFs) [1–3]. The deterministic control of CNT/CNF diameter and crystallinity is critical for bottom-up device fabrication, due to the close relationship between CNT/CNF structure/dimensions and their measured mechanical, electrical and thermal properties [4,5]. Despite substantial progress reported in the literature, it is still difficult to achieve a high level of such control, mainly due to an incomplete understanding of the growth process and the role of the catalyst. For surface-bound CVD, it was previously shown that evaporated or sputtered thin catalyst films offer accurate patterning by standard lithography techniques [3]. During the initial CVD heating stages the catalyst film coarsens, forming an island distribution, which dictates the maximal CNF/CNT dimensions. This catalyst nanostructuring process not only depends on catalyst–substrate interactions, but also on the detailed process conditions, which is often neglected when comparing CVD results.

We previously focused on plasma-enhanced (PE) CVD of CNTs/CNFs [6–9]. This allows vertical alignment and low temperature CNF growth from relatively thick (>4 nm) catalyst films. Here, we present a systematic growth study of CNTs/CNFs, analyzing the effects of plasma enhancement for very thin (<3 nm) catalyst films. We show that a reduction of the Fe/Co catalyst film thickness below 3 nm generally results in the growth of small diameter (<5 nm) multi-walled CNTs, compared to the previously described larger diameter (>40 nm), bamboo-like CNFs. For the same CVD conditions, these CNTs grow over 50 times faster with a more rapid catalyst poisoning than the CNFs. Thin Ni films trigger the growth of bundled CNTs only when pre-treated in a pure NH_3 plasma. Here, we monitor the nanostructuring of the catalyst film for a typical set of CVD conditions, demonstrating its dependency on the gas atmosphere and relating this process to the CNT/CNF growth outcome. By comparing with purely thermal CVD results, we show that DC plasma assistance can be detrimental for small diameter CNT growth.

2. Experimental details

We use polished, cleaned, n-type Si(100) wafers with a thermally grown (40–60 nm) oxide as substrates. Fe, Co and Ni

---

catalyst films are deposited by thermal evaporation (base pressure $<10^{-6}$ mbar). The film thickness is monitored in situ by a quartz crystal balance, and calibrated ex situ by atomic force microscopy (AFM, Veeco Explorer) and spectroscopic ellipsometry (J. A. Woollam Co., M-2000 V). The catalyst films are patterned by optical lithography with sub-10 μm features to facilitate CNT/CNF characterization and monitor the bare SiO_2 background.

The CNTs/CNFs are grown in a DC PECVD system in a stainless steel diffusion pumped vacuum chamber (base pressure $<10^{-6}$ mbar) with mass flow controlled (MFC) gas feeds. The substrates are transferred in air and loaded onto a resistively heated graphite stage. The temperature is continuously monitored by 3 shielded thermocouples, distributed across reference Si substrates (500 μm in thickness, equivalent to samples) and the graphite heater.

Typically, the samples are first heated in 0.6 mbar NH_3 (200 sccm, flown from a side gas inlet) for 15 min until the desired growth temperature is reached (~500–550 °C for the experiments described in this work). CNT/CNF deposition is then carried out either in a DC plasma or in purely thermal conditions (plasma off), introducing 50 sccm C_2H_2 for a gas ratio of 50:200 sccm C_2H_2/NH_3 (0.7 mbar total pressure). For plasma-assisted deposition, a DC discharge between the heater

stage (cathode) and a stainless steel anode ~3 cm above the stage is ignited by applying a fixed voltage of 600 V just a few seconds before introducing C_2H_2. The discharge current is ~20–30 mA, corresponding to <20 W plasma power, which is much lower than typically found in the literature [1,10,11].

As-evaporated and pre-treated catalyst films are characterized by AFM in tapping mode at ambient conditions. As-grown CNTs/CNFs are characterized by Scanning Electron Microscopy (SEM, LEO 1530VP FEGSEM) and High Resolution Transmission Electron Microscopy (HRTEM, Jeol JEM 4000 EX, 400 kV). For HRTEM analysis, the CNTs/CNFs are removed from the substrates and dispersed onto Cu TEM grids.

3. Results and discussion

Figs. 1 and 2 show AFM analysis of Fe films of 0.3, 1 and 5 nm nominal thickness, subject to different pre-treatment stages. Root-mean-square (RMS) roughness is measured over the whole area. The Fe films/islands are bound to immediate oxidation upon air exposure leading to an overestimation of the thickness/dimensions [12]. For convention, all film thickness values in this paper refer to the pre-oxidized value.

As-evaporated Fe films shown in Figs. 1 and 2 are characterized by a RMS surface roughness in the range of
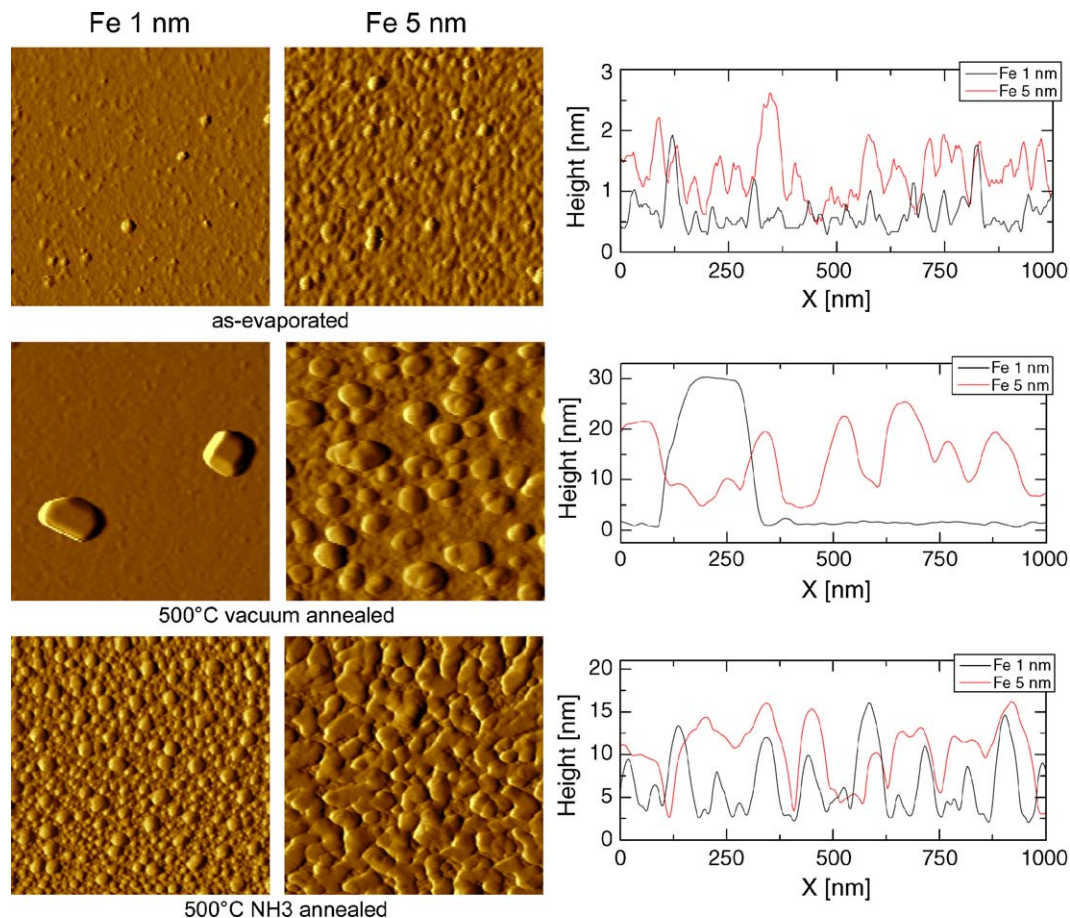
Fig. 1. (Color online) AFM analysis of 1- and 5-nm-thick Fe films subject to different pre-treatment stages: as-evaporated, annealed in vacuum ($<10^{-5}$ mbar pressure) at ~500 °C and annealed in NH_3 (0.6 mbar pressure) at ~500 °C. The section analysis show the topography profile along sample lines in the respective amplitude image. Image scan dimensions are 1×1 μm^2.

Fe 0.3 nm
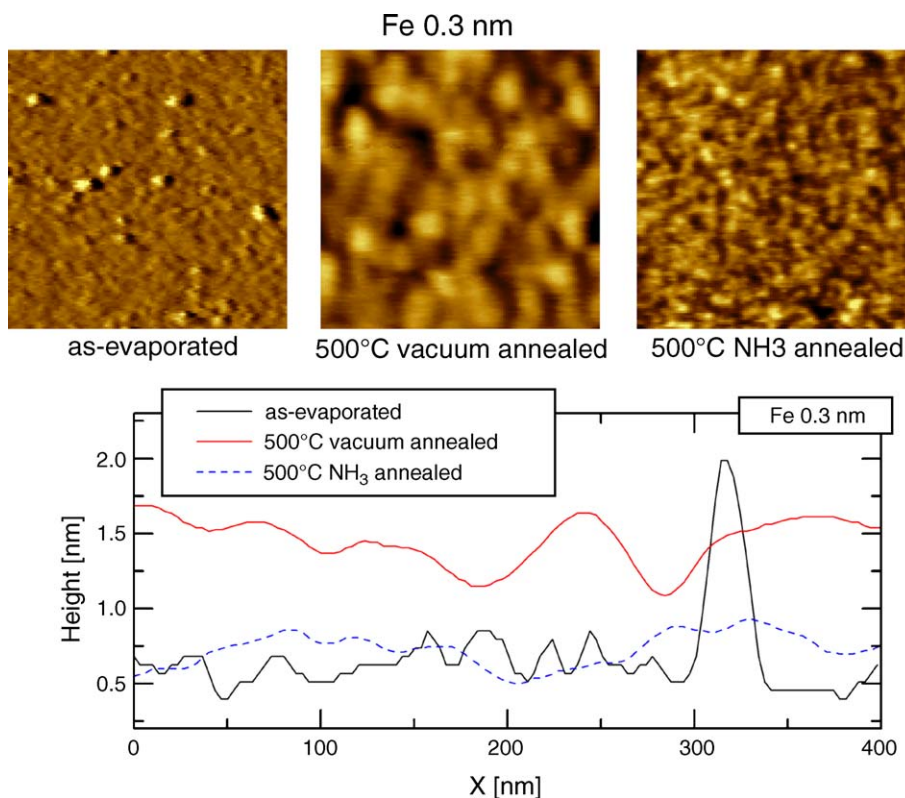
Fig. 2. (Color online) AFM analysis of 0.3-nm-thick Fe film subject to different pre-treatment stages: as-evaporated, annealed in vacuum ($<10^{-5}$ mbar pressure) at ~ 500 °C and annealed in NH_3 (0.6 mbar pressure) at ~ 500 °C. The section analysis shows the topography profile along sample lines in the respective amplitude image. Image scan dimensions are 400×400 nm^2.

0.3–0.5 nm for 0.3, 1 and 5 nm thicknesses, respectively. The 5-nm film appears continuous, whereas thinner films are discontinuous due to a Volmer–Weber film nucleation. For comparison, the RMS roughness of the oxidized Si substrate is ~ 0.15 nm.

After annealing in vacuum ($<10^{-5}$ mbar pressure) at ~ 500 °C, the solid catalyst films dewet driven by a surface and elastic energy minimization [13,14]. The SiO_2 layer prevents uncontrolled silicide formation at low deposition temperatures [15]. Depending on the detailed surface interactions, metal islands of average lateral extent w and height h form, as schematically illustrated in Fig. 3(b). The AFM analysis shows a w of ~ 40, ~ 200 and ~ 100 nm for a respective original 0.3-, 1- and 5-nm Fe thickness (Figs. 1 and 2). These values carry an uncertainty based on the convolution with the AFM tip radius of ~ 10 nm. In comparison, h is ~ 0.2 nm, ~ 30 and ~ 10 nm for vacuum annealed 0.3-, 1- and 5-nm-thick Fe films (Figs. 1 and 2). Interestingly, the annealed 1-nm film shows a much lower island density.

Annealing in pure NH_3 (200 sccm, 0.6 mbar pressure) at ~ 500 °C results in a distinctively different topography for all Fe thicknesses. The average w is ~ 30, ~ 50 and ~ 110 nm for 0.3-, 1- and 5-nm Fe films, respectively, much smaller compared to the vacuum annealed films (Figs. 1 and 2). The island height is from ~ 0.1, ~ 5 and ~ 10 nm, giving a high island density for the thinnest, NH_3-annealed Fe films.

In literature, the reported pre-growth annealing atmosphere often varies, making a detailed comparison difficult. Also, the metal island anisotropy, expressed by w and h, is often neglected. Nerushev et al. [16] report an average w of 26 nm and h of 2–3 nm for islands formed from 1- to 2-nm Fe films after treatment at 750 °C in a H_2/Ar gas mixture. In the case of vacuum annealed films, Wang et al. [17] report structures of ~ 10–15 nm and a RMS roughness of 0.4–0.5 nm for 0.3–0.5 nm Fe films annealed at 850 °C, while Wei et al. [18] calculate an average island size of <10 nm upon annealing of a 5-nm Fe film at 660 °C.
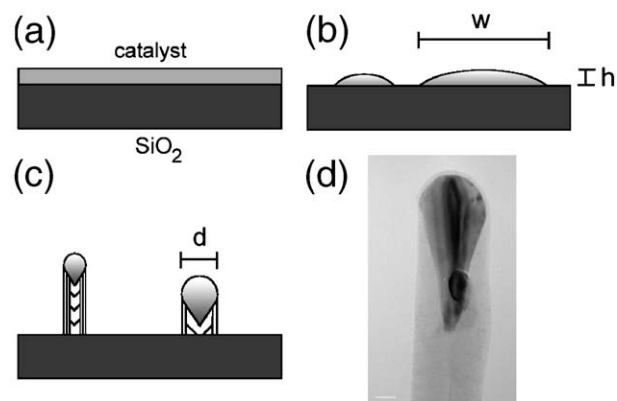
Fig. 3. Schematic of the CNT/CNF growth mechanism. The initial thin catalyst film (a) is heated up to the desired temperature and splits up into islands (b). Nanotubes grow as the hydrocarbon precursor is fed into the chamber (c), and a HRTEM image shows an example of CNF grown with tip-growth mechanism (d, scale bar: 20 nm).

Fig. 4 compares thermally and DC PECVD-grown CNTs from 0.3-, 1-, 2- and 5-nm-thick Fe films at ∼550 °C. We observe purely thermal CNT growth only for ≤2-nm-thick Fe films. In contrast, plasma enhancement enables CNF nucleation for thicker catalyst films (Fig. 4(h)) [19]. Wei et al. reported on a critical catalyst film thickness beyond which no thermal CNT growth was observed [18]. On the other hand, the same authors observed CNT growth over the entire catalyst thickness range under DC plasma conditions [18]. We observe similar effects here, however, we would like to emphasize that for our experiments this refers to isobaric conditions.

When comparing different CVD conditions, the actual CNT/CNF growth process has to be separated from the effects of catalyst film coarsening. Regarding catalyst pre-treatment conditions, our previous studies showed that ∼2–5 s of pure NH_3 plasma pre-treatment (to simulate the film conditions just prior to a DC PECVD standard run) affects the surface topography of the NH_3-annealed Fe film [19]. A major effect of the plasma is to etch the catalyst surface, leading to the disappearance of the smallest catalyst islands. This in turn affects the resulting CNT density. Fig. 4(a) shows CNTs so closely packed that SEM can hardly resolve them, whereas CNT forests grown under PECVD conditions (Fig. 4(b)) show less homogeneity and a lower density. For 0.3-nm-thick Fe films, the difference in CNT density (Fig. 4(a,b)) is much higher than for thicker Fe films (Fig. 4(c–f)), because the island size increases as film thickness increases, and the etching effect of the NH_3 plasma is less influential on larger islands. For Fe films ≤0.1 nm, we observe sparse growth under purely thermal conditions, whereas no growth is seen for PECVD due to an almost complete removal of the catalyst metal.

HRTEM analysis (Fig. 5) shows that, in the case of 2-nm-thick Fe catalyst films, DC plasma as well as thermally grown CNTs consist of 2–3 walls and tend to bundle. The diameter distributions are similar (2.6–4.6 nm), with ∼3.5 nm average diameter. However, the CNT walls appear straighter and more parallel for the thermally grown sample. Plasma bombardment during CNT growth can introduce lattice defects, causing bending and alterations of the nanotube diameter during growth. Reactive NH_x species can not only etch the catalyst particle but also as-grown small diameter nanotube shells. The used plasma conditions seem too aggressive for the nucleation of pristine quality few-walls CNTs. As a consequence, CNT bundles appear neater and more regular for thermal CVD. It should be noted that here CNT alignment is a proximity effect [2] and is not field-induced as for DC PECVD of larger diameter CNFs [20]. At lower temperatures (∼450 °C), differences in yield from thermally and DC PECVD-grown CNTs from thin Fe layers are dramatically enhanced.

It is important to note that for a similar catalyst pre-treatment, but different thermal CVD growth conditions (such as pressure and hydrocarbon dilution), we find <0.5 nm Fe films to nucleate SWNT mats at temperatures as low as 350 °C [21]. We do not observe SWNT growth under comparable DC PECVD
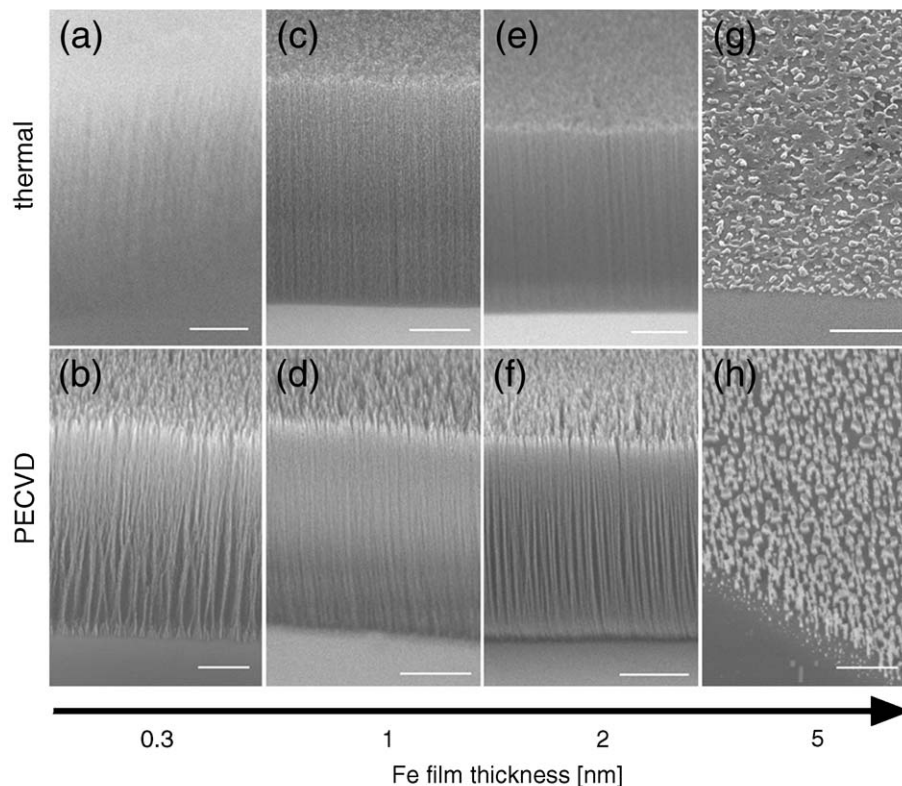
Fig. 4. SEM images of CNTs grown from 0.3-, 1-, 2- and 5-nm-thick Fe films under purely thermal and DC PECVD conditions. Growth conditions were: ∼550 °C and 1:4 C_2H_2/NH_3 gas mixture. For DC PECVD-grown CNTs, a 600 V DC bias was applied. Scale bars are: 2 μm (a, b, g), 5 μm (c–f), 1 μm (h).
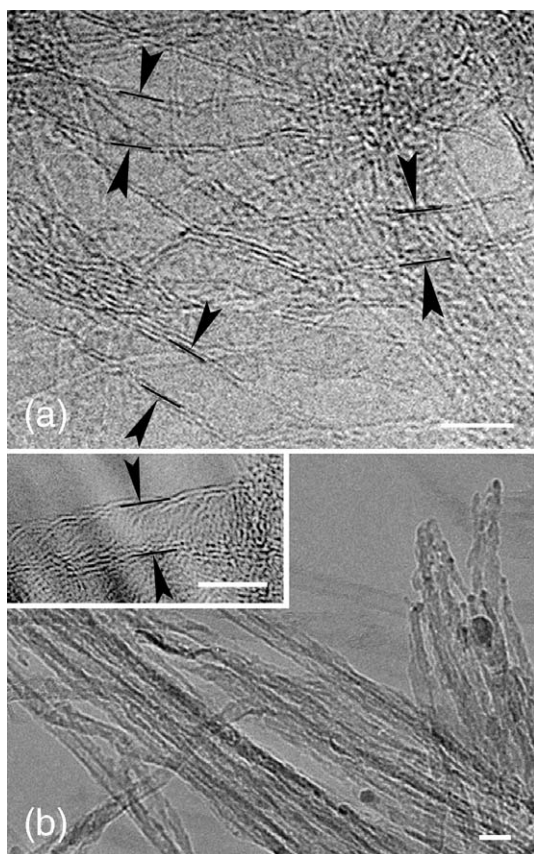
Fig. 5. HRTEM analysis of thermally (a) and DC PECVD-grown (b) CNTs catalyzed from 2-nm-thick Fe films. Scale bars are: 5 nm (a), 20 nm (b), 5 nm (inset).

conditions. SWNTs are prone to etching in H_2 and NH_3-rich plasmas. Other groups reported SWNT nucleation with the help of remote plasmas [22,23] or using a physical barrier to eliminate direct plasma bombardment of the substrate [17].

To underline the important role of the catalyst pre-treatment, we find that pre-treating >1-nm-thick Ni catalyst films in a pure NH_3 plasma enables purely thermal growth of bamboo-like, thick CNFs at temperatures as low as 200 °C [24]. Plasma etching can result in higher nucleation density for CNTs/CNFs growth especially at low temperatures, as previously reported [1,6,25]. Catalyst clusters can form from polycrystalline metal by a preferential etching at grain boundaries. A heavy plasma pre-treatment has been found to be beneficial to trigger CNF growth by PECVD in thick (10 nm) Fe catalyst films, restructuring them after annealing into 100–200 nm diameter islands [26].

In our previous study, we found that, at ~550 °C, <3 nm Fe/Co films trigger the growth of 2–3 walls, small diameter (<5 nm), bundled CNTs in DC PECVD conditions, in contrast to larger diameter (>40 nm), shorter CNFs grown from thicker films [19]. However, we found that thin Ni films need a pre-treatment process in order to achieve similar growth results. In contrast to standard depositions where C_2H_2 is fed shortly after plasma ignition, thin Ni films have been subject an additional 5 min pre-etching in a pure NH_3 plasma (<15 W power), thereby resulting in CNT bundles

similar to those found for Fe and Co films of comparable thickness [19]. If thermal annealing does not lead to a catalyst restructuring suitable for CNT growth, plasma etching can activate these changes in the catalyst surface topography. In the case of thin Co films, plasma pre-treatment enhances the nucleation of smaller diameter CNTs, while for Fe, plasma pre-treatment seems to have no effects other than enabling CNT growth for nominally thicker films.

As schematically shown in Fig. 3, the relation between the CNT/CNF diameter d (Figs. 4 and 5) and the initial catalyst island dimensions w and h (Figs. 1 and 2) strongly depends on the degree of catalyst island reshaping during CVD. The restructuring of the metal catalyst particle is continuous during growth depending on the formation of graphene on its surface [27]. Post-growth HRTEM typically shows catalyst particles elongated along the tube axis for tip-growth (Fig. 3(d)) [28,29]. The volume of the catalyst particle can also get consumed by plasma etching during PECVD. Furthermore, for tip-growth not all of the catalyst metal might be lifted off the support based on interface reactions. Generally, we see that thicker Fe films result in larger catalyst islands nucleating larger diameter CNT/CNFs ((Figs. 1, 2 and 4)) [19]. However, our AFM analysis shows that the metal coarsening depends on the atmosphere. We find a catalyst pre-treatment in vacuum not to yield any thermal CNT/ CNF growth for many conditions. Figs. 1 and 2 suggest that this is due to larger catalyst island dimensions for the vacuum anneal. On the other hand, we observe that for Fe films ≤2-nm thickness, annealing in NH_3 appears to enhance the growth of dense forests of bundled, small diameter CNTs. Therefore, care has to be taken when comparing the "efficiency" of different CVD conditions even when nucleating from the same Fe film thickness and support, since the catalyst coarsening is representative of the conditions, as well and the actual CVD growth will not (unlike commonly assumed) start from the same catalyst size distribution. For surface-bound CVD of small diameter CNTs, especially SWNTs, the controlled catalyst
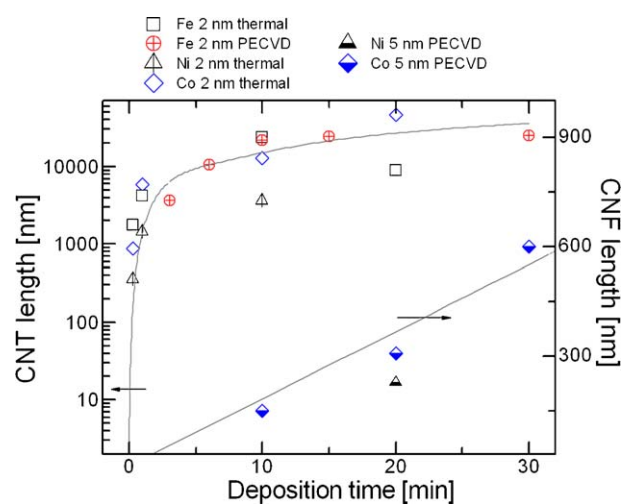
Fig. 6. (Color online) Growth saturation plot of CNTs grown under purely thermal and DC PECVD from 2-nm-thick catalyst films, compared with CNFs grown from thicker (5 nm) catalyst films under DC PECVD conditions. Growth temperatures are ~550 °C for CNTs (left axis) and ~450 °C for CNFs (right axis).
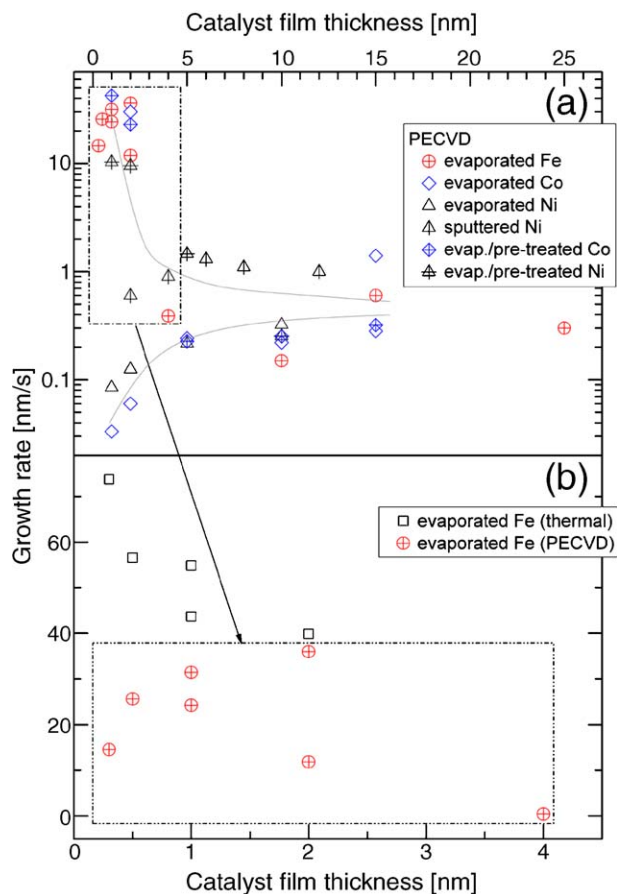
Fig. 7. (Color online) Variation of average CNT/CNF growth rate as a function of catalyst thin film thickness for Fe, Co and Ni-catalyzed CNT/CNF samples grown in DC PECVD conditions (a), and comparison between CNTs grown from Fe only, in purely thermal and DC PECVD conditions (b).

splitting is a key factor for diameter control and thus control over some of their properties.

Fig. 6 shows the growth saturation behaviour of the two different CNT and CNF growth regimes. Generally, CNT/CNF growth saturation is due to catalyst poisoning, which is believed to be caused by the progressive formation of an amorphous carbon layer at the catalyst surface [30]. CNTs grown in purely thermal and DC PECVD conditions from 2-nm-thick catalyst films are found to have a very high growth rate (>70 nm/s) but they saturate within the first 1–2 min of growth, after which the growth rate lowers considerably (<20 nm/s). In contrast, 5-nm-thick catalyst films tend to nucleate thick CNFs with a constant growth rate, for up to at least up to 60 min (not shown in the plot), under DC PECVD conditions only (Fig. 4(h)), since these films are too thick to trigger CNT/CNF thermal growth (Fig. 4 (g)). Thin CNTs nucleate from small catalyst particles, characterized by a smaller active surface, which is likely to poison more quickly compared to bigger clusters catalyzing the growth of thick CNFs. It is surprising, however, that thermal CVD and DC PECVD of thin CNTs exhibit a similar saturation behavior, as a reactive plasma atmosphere could potentially remove poisoning amorphous carbon. In that regime and with the conditions used, the DC discharge looses the advantages of its aggressive etching behavior.

From the similar saturation of thermally and DC PECVD-grown CNTs from 2-nm-thick Fe films (Fig. 6) and the assumption that this similarity is preserved for thicknesses in the 0.3–2-nm range (as Fig. 4 indicates), we can plot the growth rate vs. film thickness for the different growth conditions (Fig. 7). Fig. 7(b) shows how the DC plasma enhancement can be detrimental for small diameter CNT growth.

4. Conclusions

In conclusion, the effects of pre-treatment stages and growth conditions on ultra-thin, evaporated catalyst films for CNT/CNF growth have been discussed. The catalyst film splitting was mapped for our growth conditions, clearly demonstrating its dependency on the gas atmosphere and its dominating effect on the CNT/CNF diameter distribution. Whereas essential for CNF nucleation from thick catalyst films, DC plasma assistance was found to be ineffective in preventing catalyst poisoning, detrimental to sample homogeneity and to induce structural defects for small diameter CNTs.

Acknowledgements

References

[1] Z.F. Ren, Z.P. Huang, J.W. Xu, J.H. Wang, P. Bush, M.P. Siegal, P.N. Provencio, Science 282 (1998) 1105.
[2] S.S. Fan, M.G. Chapline, N.R. Franklin, T.W. Tombler, A.M. Cassell, H.J. Dai, Science 283 (1999) 512.
[3] J. Kong, H.T. Soh, A.M. Cassell, C.F. Quate, H.J. Dai, Nature 395 (1998) 878.
[4] M. Terrones, Annu. Rev. Mater. Res. 33 (2003) 419.
[5] P. Avouris, J. Appenzeller, R. Martel, S.J. Wind, Proc. IEEE 91 (2003) 1772.
[6] S. Hofmann, C. Ducati, B. Kleinsorge, J. Robertson, Appl. Phys. Lett. 83 (2003) 135.
[7] S. Hofmann, C. Ducati, B. Kleinsorge, J. Robertson, Appl. Phys. Lett. 83 (2003) 4661.
[8] M. Cantoro, S. Hofmann, B. Kleinsorge, G. Csanyi, M.C. Payne, A.C. Ferrari, J. Robertson, Proc. of XVIII International Winterschool on Electronic Properties of Novel Materials, Kirchberg (Austria), 6–13 March 2004, p. 81.
[9] S. Hofmann, G. Csanyi, A.C. Ferrari, M.C. Payne, J. Robertson, Phys. Rev. Lett. 95 (2005) 036101.
[10] A.V. Melechko, V.I. Merkulov, D.H. Lowndes, M.A. Guillorn, M.L. Simpson, Chem. Phys. Lett. 356 (2002) 527.
[11] C. Ducati, I. Alexandrou, M. Chhowalla, G.A.J. Amaratunga, J. Robertson, J. Appl. Phys. 92 (2002) 3299.
[12] L. Gan, R.D. Gomez, C.J. Powell, R.D. McMichael, P.J. Chen, W.F. Egelhoff, J. Appl. Phys. 93 (2003) 8731.
[13] M. Liehr, H. Lefakis, F.K. Legoues, G.W. Rubloff, Phys. Rev. B 33 (1986) 5517.
[14] E. Jiran, C.V. Thompson, J. Electron. Mater. 19 (1990) 1153.
[15] A. Wawro, S. Suto, R. Czajka, A. Kasuya, Phys. Rev. B 67 (2003) 195401.
[16] O.A. Nerushev, S. Dittmar, R.E. Morjan, F. Rohmund, E.E.B. Campbell, J. Appl. Phys. 93 (2003) 4185.
[17] Y.Y. Wang, S. Gupta, R.J. Nemanich, Appl. Phys. Lett. 85 (2004) 2601.

[18] Y.Y. Wei, G. Eres, V.I. Merkulov, D.H. Lowndes, Appl. Phys. Lett. 78 (2001) 1394.

[19] S. Hofmann, M. Cantoro, B. Kleinsorge, C. Casiraghi, A. Parvez, J. Robertson, C. Ducati, J. Appl. Phys. 98 (2005) 034308.

[20] C. Bower, W. Zhu, S.H. Jin, O. Zhou, Appl. Phys. Lett. 77 (2000) 830.

[21] M. Cantoro, S. Hofmann, V. Scardaci, A. Parvez, S. Pisana, C. Ducati, A. Blackburn, A.C. Ferrari, J. Robertson (submitted for publication).

[22] Y.M. Li, D. Mann, M. Rolandi, W. Kim, A. Ural, S. Hung, A. Javey, J. Cao, D.W. Wang, E. Yenilmez, Q. Wang, J.F. Gibbons, Y. Nishi, H.J. Dai, Nano Lett. 4 (2004) 317.

[23] G.F. Zhong, T. Iwasaki, K. Honda, Y. Furukawa, I. Ohdomari, H. Kawarada, Jpn. J. Appl. Phys. 44 (2005) 1558.

[24] M. Cantoro, S. Hofmann, et al. (in preparation).

[25] Z.P. Huang, J.W. Wu, Z.F. Ren, J.H. Wang, M.P. Siegal, P.N. Provencio, Appl. Phys. Lett. 73 (1998) 3845.

[26] H. Cui, O. Zhou, B.R. Stoner, J. Appl. Phys. 88 (2000) 6072.

[27] S. Helveg, C. Lopez-Cartes, J. Sehested, P.L. Hansen, B.S. Clausen, J.R. Rostrup-Nielsen, F. Abild-Pedersen, J.K. Norskov, Nature 427 (2004) 426.

[28] H.T. Cui, X.J. Yang, M.L. Simpson, D.H. Lowndes, M. Varela, Appl. Phys. Lett. 84 (2004) 4077.

[29] C. Ducati, I. Alexandrou, M. Chhowalla, J. Robertson, G.A.J. Amaratunga, J. Appl. Phys. 95 (2004) 6387.

[30] R.T.L. Baker, M.A. Barber, Chemistry and Physics of Carbon, Dekker, New York, 1978.